Validation of an automated method to quantify stress-induced ischemia and infarction in rest-stress myocardial perfusion SPECT.

Fransson, Helen; Ljungberg, Michael; Carlsson, Marcus; Engblom, Henrik; Arheden, Håkan; Heiberg, Einar

Published in:
Journal of Nuclear Cardiology

DOI:
10.1007/s12350-014-9863-y

2014

Title Validation of an automated method to quantify stress-induced ischemia and infarction in rest-stress myocardial perfusion SPECT

Authors Helen Fransson[1]PhD, Michael Ljungberg[2]PhD, Marcus Carlsson[1]MD PhD, Henrik Engblom[1]MD PhD, Håkan Arheden[1]MD PhD, Einar Heiberg[1] PhD

Author affiliation [1]Department of Clinical Physiology and Nuclear Medicine, Lund University, Lund University Hospital, Sweden, [2]Department of Medical Radiation Physics, Clinical Sciences, Lund, Lund University, Lund, Sweden

Corresponding Author Einar Heiberg, Department of Clinical Physiology, Lund University Hospital, SE-221 85 Lund, Sweden, Tel: +46-46-17 33 40 Fax: +46-46-15 17 69, einar.heiberg@med.lu.se

Financial support Swedish Heart Lung Foundation, Lund University Faculty of Medicine, the Swedish Research Council, Swedish Knowledge Foundation, and the Region of Scania.

Abstract

Background: Myocardial perfusion SPECT (MPS) is one of the frequently used methods for quantification of perfusion defects in patients with known or suspected coronary artery disease. This article describes open access software for automated quantification in MPS of stress-induced ischemia and infarction and provides phantom and in vivo validation.

Methods and Results: A total of 492 patients with known or suspected coronary artery disease underwent both stress and rest MPS. The proposed perfusion analysis algorithm (Segment) was trained in 140 patients and validated in the remaining 352 patients using visual scoring in MPS by an expert reader as reference standard. Furthermore, validation was performed with simulated perfusion defects in an anthropomorphic computer model. Total perfusion deficit (TPD, range 0-100), including both extent and severity of the perfusion defect, was used as the global measurement of the perfusion defects.

Mean bias±SD between TPD by Segment and the simulated TPD was 3.6±3.8 (R^2=0.92). Mean bias±SD between TPD by Segment and the visual scoring in the patients was 1.2±2.9 (R^2=0.64) for stress-induced ischemia and -0.3±3.1 (R^2=0.86) for infarction.

Conclusion: The proposed algorithm can detect and quantify perfusion defects in MPS with good agreement to expert readers and to simulated values in a computer phantom.

Introduction

Myocardial perfusion SPECT (MPS) is an established non-invasive imaging technique for detection and quantification of myocardial perfusion defects in patients with coronary artery disease (CAD) (1 , 2). Comparison of rest MPS to stress MPS enables quantification of stress-induced ischemia. By using normal limits of perfusion, MPS also provides the ability to quantify infarction (3). The interpretation of MPS images is routinely performed by visual reading supported by automated analysis software packages. The most common approach in current software packages to perform quantification of perfusion defects is to compare to a normal perfusion database (4-7). The comparison is traditionally performed for the rest and the stress tomographic sections separately, and thereafter the results are compared. One limitation with this approach is that no direct alignment of stress and rest MPS is performed. Another limitation is that the comparison depends on the two different left ventricular (LV) segmentations, which can differ significantly between the paired MPS images, in particular in the basal region of the LV. These limitations can confound the assessment of perfusion defects due to comparison of regions located in different parts of the myocardium. Furthermore, even when rest and stress tomographic sections are perfectly aligned, the comparison to normal limits is based on inter-patient comparison. This may cause true differences in perfusion to go undetected since the images are not compared directly.

A recent study has shown higher diagnostic performance for stress-induced ischemia by using voxel-based image registration and direct comparison of counts between rest and stress images, compared to the standard method of separate analysis of rest and stress images (8). Furthermore, incorporating regional myocardial function in automatic perfusion analysis has shown higher accuracy for detection of myocardial infarction compared to only including myocardial counts in the analysis (9). Therefore, the aim of this study was to combine voxel-based image registration of rest and stress images with regional myocardial function at rest to develop a new freeware method for quantification of both stress-induced ischemia and infarction in MPS images.

Materials and Methods

Study population and design

All patients provided written informed consent to participate in the study and the study was approved by the regional ethics committee. Patients referred for MPS imaging during 2008-2011, due to known or suspected coronary artery disease, with rest and stress MPS at the same day were considered for enrollment. A training set was designed by assessing the myocardial perfusion by experienced observers, and then include a control group of 90 patients with a normal perfusion scan and a CAD group of 50 patients with perfusion defects. Inclusion criteria for the control group were normal global systolic function (Ejection fraction (EF) > 50). Exclusion criteria for the control group were history of CAD, atrial fibrillation, arrhythmia, LV bundle branch block, heart failure, pacemaker, death or valvular heart disease, within two years or prior to the MPS imaging. The remaining patients, both with and without perfusion defects, formed a test set of 352 patients. The patient characteristics for both the training set and the test set are shown in Table 1.

Myocardial Perfusion SPECT Acquisition and Analysis

Myocardial perfusion SPECT was performed according to established clinical one day protocols using a dual head camera GE Ventri (GE Healthcare, Waukesha Wisconsin, USA). Gated MPS images were acquired

at stress and rest for each patient, after injection with ^{99m}Tc tetrofosmin (Myoview, Amersham Health, Buckinghamshire, UK). Injection at stress was 4 MBq ^{99m}Tc tetrofosmin per kg bodyweight, and at rest approximately 12 MBq ^{99m}Tc tetrofosmin per kg bodyweight. Patients were stressed using maximal exercise test, adenosine, or a combination of the two. Dobutamine was used when maximal exercise test and adenosine were contra-indicated. The patient was placed in supine position and imaged in steps of 3 degrees using a 64x64 matrix with a pixel size of 6.4x6.4 mm^2 and a slice thickness of 6.4 mm. Images were gated to a simultaneously acquired electrocardiogram using 8 frames per cardiac cycle. Image acquisition time was approximately 12 minutes. According to clinical practice at Lund University Hospital, iterative reconstruction using ordered subset expectation maximization (OSEM) with two iterations and ten subsets was performed with a low-pass Butterworth filter. For stress the cutoff frequency was set to 0.4 of Nyquist and an order of 10, and for rest the cutoff frequency was set to 0.52 of Nyquist and an order of 5. No attenuation or scatter correction was applied. Short-axis images were reconstructed semi-automatically with manual adjustments using the software package Cedars QGS/QPS (Xeleris version 3, GE Healthcare). Reconstructed MPS images were loaded into the software package Segment (version 1.9 Medviso AB, Lund, Sweden).

Computer Phantom Data

As a complement to the patient validation, the automatic perfusion analysis algorithm was validated by simulated MPS images by a computer phantom. The simulated MPS projection data were generated by using the XCAT mathematical anthropomorphic phantom (10) together with the Monte Carlo based simulation program SIMIND (11). In the simulation, the SPECT system parameters were set according to the clinical one day protocol, as described above, and realistic noise levels were created by adding Poisson noise. Identical camera parameters were used to match as close as possible to realistic clinical situations. The simulation was performed in both male and female geometry, with varying LV geometries and varying sizes, location and severity of the perfusion defect. A total of 48 sets of tomographic sections (24 male, 24 female) were simulated, 12 with normal perfusion and 36 with various perfusion defects. The phantom projection data including effects from non-homogeneous photon attenuation, scatter and the collimator response, were reconstructed as described above for the patient data. Finally, the phantom data were loaded into the software packages Segment and QPS for automatic LV segmentation and perfusion analysis. Figure 1 shows one of the paired simulated MPS images with an overlaid LV segmentation by Segment.

Visual Perfusion Scoring

The manual perfusion analysis of the MPS images was performed in the software package Segment. The LV was automatically segmented as previously described (12), with manual corrections if necessary. The LV myocardia were automatically divided into 17 segments using the standard division of the LV (13), and each segment was scored manually for tracer uptake and presence of infarction, respectively. The manual interpretation to detect myocardial infarction using gated MPS was recently validated by cardiac magnetic resonance imaging, with high sensitivity and specificity for detecting infarction (14). Figure 2 illustrates the interface used in the scoring process. The scoring was performed by an experienced physician (MD, PhD) specialized in nuclear cardiology with 12 years of clinical and scientific experience with MPS. The observer was blinded to patient information and the results from the automatic perfusion analysis. To determine interobserver variability, two additional observers performed perfusion scoring in 40 MPS images, randomly chosen from the test set. The second and the third observer were blinded to the scoring by the first observer. The second and third observers are both experienced physicians (MD, PhD) specialized in nuclear cardiology with 10 and 20 years of experience with MPS, respectively.

A difference score was obtained by taking the difference between the stress and rest tracer uptake score in each of the 17 segments of the LV. Single

segments with a score of 1, which were not contiguous with segments of scores>0, were assigned a score of 0. By summation of the difference score a summed difference score (SDS) was obtained. Stress-induced ischemia was defined as a SDS $\geq$ 2, as previously established (8). A summed rest score (SRS) was obtained by summation of the tracer uptake scores of those LV segments in the rest image where the infarct score was equal to 2. Myocardial infarction was defined by one or more regions with an infarct score of 2. For comparison with the automatic defect quantification, the summed scores were converted to percent of the total myocardium with defects by multiplying the summed scores by 100 and dividing by 64 (the maximum score). Those converted scores were labeled SD% and SR%, for stress-induced ischemia and infarction, respectively (15).

Automatic Perfusion Analysis

The proposed algorithm for automatic perfusion analysis in MPS images is implemented in the freely available software Segment (http://segment.heiberg.se). In this study, Segment was used for both manual and automatic perfusion analysis (16). The LV was automatically segmented in both the gated and ungated tomographic sections as previously described (12), with manual corrections if necessary. The proposed automatic perfusion analysis algorithm then segments and quantifies the perfusion defects. The perfusion analysis algorithm starts by count

normalization and image registration of the ungated rest and stress tomographic sections. The normalization aims to normalize to similar maximum count in each image slice. The registration is an affine transformation aiming to have a direct comparison of voxels between the rest and the stress tomographic sections. The normalization and registration processes are described in more detail in the Appendix. Regional wall thickening was calculated from the LV segmentation in the rest gated tomographic sections, by increase in distance between computed LV walls. The wall thickening for each voxel was thereafter assigned to each myocardial voxel in the rest ungated tomographic sections. The rest and stress myocardial counts, the rest-stress counts change, and the rest wall thickening were used as features to classify the myocardium as normal, stress-induced ischemia or infarction, by a probabilistic classification algorithm. The classification was performed by a Naive Bayes classifier, as described in more detail in the Appendix. Finally, the perfusion defect segmentation was refined by considering *a priori* knowledge of perfusion defects propagation within the myocardium. The refinement of the perfusion segmentation is described in more detail in the Appendix. From the perfusion defect segmentation the perfusion defect was quantified by calculating the extent and total perfusion deficit (TPD) of the defect. Extent was presented as percentage of the LV. The TPD measure includes both extent and severity of the perfusion defect, and is a continuous value

ranging from 0 (no perfusion defect) to 100 (severe perfusion defect in the whole LV). TPD is calculated by(17)

$$TPD = 100 \times \frac{\sum_{i=0}^{N} score_i}{N}$$

where *N* was the total number of voxels within the myocardium and *score* was a continuous value assigned to each myocardial voxel ranging from 0 (no defect) to 1 (severe defect). The TPD measurement for stress-induced ischemia was calculated by the count difference between stress and rest within the segmented stress-induced ischemia, and was labeled D-TPD. The TPD measurement for infarction was calculated for the segmented perfusion defect in the rest image and was labeled R-TPD.

Perfusion Analysis by QPS

For comparison, the MPS short-axis images were also loaded into the software package Quantitative Perfusion SPECT (QPS, version Suite2009; Cedars-Sinai Medical Centre, Los Angeles, CA) (15). The LV was automatically segmented by the program, with manual corrections of the LV segmentation when necessary. QPS then automatically quantifies the perfusion defect by TPD in the rest and stress tomographic sections separately using the vendor provided sex specific normal database. The TPD measurement for stress-induced ischemia was calculated by the difference between stress TPD and rest TPD (15), and labeled D-TPD. The

TPD measurement in the rest tomographic sections was used as assessment of infarction and labeled R-TPD.

Statistical analysis

Values are presented as mean ± SD unless otherwise stated. The diagnostic accuracy for TPD by Segment for detection of stress-induced ischemia and infarction, respectively, compared to visual scoring was obtained from analysis of receiver operating characteristic (ROC) curves (18). Sensitivity, specificity, accuracy as well as positive and negative predictive values with corresponding standard errors were calculated using standard definitions. Inter-class correlation (ICC) was used for calculating interobserver variability. Pearson's linear regression analysis was performed to calculate the relationship between two data sets where normal distribution could be assumed. Student's paired t-test was performed to test statistical significance of differences between continuous variables. Differences with p-values below 0.05 were considered statistically significant. All statistical analyses except area under curve (AUC) calculation were performed in Matlab (R2011a, MathWorks). The AUC was calculated using SPSS (version 21, IBM Corporation).

Results

Computer Phantom Study

Figure 3 illustrates the relationship between the simulated TPD for the computer phantom and the TPD calculated by Segment and QPS. For the data sets with normal perfusion, 11 out of 12 studies were quantified as TPD = 0 by Segment, and 5 out of 12 studies were quantified as TPD = 0 by QPS.

Patient Study

The experts' classifications in the test set with 352 patients showed stress-induced ischemia and / or infarction in 38 % of the patients. Manual correction of the LV segmentation was performed in 5 % (18 out of 352) of the patients in the test set for Segment and 3 % (9 out of 352) for QPS. Interobserver variability between the three observers were for SR% ICC = 0.97 and for SD% ICC = 0.77. The bias and SD between observer 1 and the two other observers are presented in Table 2. Figure 4 illustrates the relationship between the TPD calculated by Segment and the visual scoring. By excluding the wall thickening information in the automatic perfusion analysis in Segment, the bias between TPD calculated by Segment and the visual scoring was unchanged, compared to when the wall thickening information was included in the automatic analysis. Figure 5 illustrates the relationship between the TPD calculated by QPS and the visual scoring. For

the stress-induced ischemia quantification, the bias was not significantly different between Segment and QPS ($p = 0.18$), whereas the variability was significantly lower for Segment than for QPS ($p < 0.05$). For the infarct quantification, the bias and variability was significantly lower for Segment than for QPS ($p < 0.05$). Figure 6 illustrates the distribution of the TPD measurement by the automatic analysis algorithms for patients with normal perfusion defined by the expert reader. For those patients with normal stress-rest difference perfusion (SD% = 0), Segment and QPS also assessed D-TPD = 0 in 48 % and 45 % of the cases, respectively. By using D-TPD < 5 (19) as the threshold for normal perfusion, Segment and QPS assessed normal perfusion in 90% and 86% of the cases, respectively. For those patients with normal rest perfusion (SR% = 0), Segment and QPS also assessed R-TPD = 0 in 87 % and 14 % of the cases, respectively. By using R-TPD < 5 (19) as the threshold for normal perfusion, Segment and QPS assessed normal perfusion in 99% and 70% of the cases, respectively. Table 2 presents the comparison of bias and variance for the two second observers and the two automatic algorithms, by using observer one as reference standard. Figure 7 illustrates the results from the image registration and perfusion defect segmentation by Segment in one patient with both stress-induced ischemia and infarction. Figure 8 shows the resulting ROC curves of diagnostic accuracy for TPD by Segment to detect stress-induced ischemia and infarction, respectively, when using manual scoring as

reference standard. The area under the curve was 0.87 to detect stress-induced ischemia, and 0.91 to detect infarction. The ROC curves of diagnostic accuracy for TPD by QPS to detect stress-induced ischemia and infarction, respectively, are found in Supplemental file 1.The area under the curve for QPS was 0.64 to detect stress-induced ischemia, and 0.89 to detect infarction. Table 3 present the result from the ROC analysis for both Segment and QPS.

Discussion

The major findings of this study was that the proposed perfusion analysis algorithm can detect and quantify stress-induced ischemia and infarction in MPS with good agreement to expert readers, in patients with varying degrees of stress-induced ischemia and infarction. Furthermore, the automatic perfusion defect quantification shows good agreement to simulated values by a computer phantom.

Diagnostic performance

The bias against expert readers was for infarct quantification lower for the proposed analysis algorithm in Segment than for QPS, see Figure 4 and 5. For stress-induced ischemia, the bias did not differ between the two automatic algorithms. For the patients with normal stress-rest difference perfusion, the two algorithms showed similar performance (left panels in Figure 6). For the patients with normal rest perfusion, however, Segment showed R-TPD = 0 in 87% of the cases (R-TPD < 5 in 99% of the cases) whereas QPS showed R-TPD = 0 in only 14% of the cases (R-TPD < 5 in 70% of the cases), as shown in the right panels in Figure 6. As presented in Table 2, the automatic algorithms performance is comparable with the performance between observers.

The results of this study showed diagnostic performance similar to previous studies validating quantification of perfusion defects by automatic algorithms with manual interpretation of MPS images as reference standard (20-22). Lomsky et al. (20) reported a sensitivity and specificity for detection of stress-induced ischemia of 0.90 and 0.85, respectively, and for detection of infarction 0.89 and 0.96, respectively, for a patient population with ischemia in 17 % and infarction in 9 % of the patients. Garcia et al. (21) reported a sensitivity and specificity for detection of CAD of 0.83 and 0.73, respectively, for a patient population with CAD in 73 % of the patients. Johansson et al. (22) evaluated three software packages for detection of CAD and reported an area under the curve of 0.87, 0.82 and 0.76 and a sensitivity and specificity in the range of 0.79-0.87 and 0.42-0.79, respectively, for a patient population with CAD in 30 % of the patients. However, when comparing results from different studies, it is important to consider that the criteria used to determine diagnostic accuracy (sensitivity and specificity) are a function of the prevalence and severity of CAD in the population, which varied between the study populations above.

As showed by a previous study (23), detection of CAD with support by automatic perfusion analysis improved the consistency between observers. This illustrates one benefit with the support of automatic perfusion analysis,

since physicians may be able to use the second opinion from the automatic perfusion analysis to improve their clinical accuracy.

Computer Phantom Study

The validation of the proposed automatic algorithm by the computer phantom showed good agreement with simulated values (Figure 3). Eleven of the twelve data sets with normal perfusion were correctly quantified as no perfusion defect by Segment. For QPS, five of the twelve normal data sets were correctly quantified as no perfusion defect. A slight overestimation of the perfusion defect was found for both of the automated algorithms.

Automatic Perfusion Algorithm

The major algorithmic strengths of the developed method are 1) quantification of both stress-induced ischemia and infarction, 2) inclusion of regional myocardial function at rest to assess infarction, and 3) image registration enables direct comparison between rest and stress image data, making each person their own control. Image registration for MPS images has been applied previously for comparison to normal databases (6, 24) and for alignment of paired rest and stress images (8). The previous method (8) for alignment of paired rest and stress images performs a voxel-based co-registration, followed by comparison to a bullseye normal model of reversibility. However, this method only quantifies stress-induced ischemia

and does not quantify infarction. A method for quantification of both stress-induced ischemia and infarction was proposed by Lomsky et al. (20). This method uses an active shape model to segment the LV and obtain myocardial counts and regional myocardial function values. These values are then used as features in an artificial neural network to quantify perfusion defects. In this previous study, incorporation of regional myocardial function in the analysis resulted in higher accuracy for detection of infarction, compared to only include myocardial counts in the analysis (9). To our knowledge, the proposed method is the first method that combines voxel-based co-registration of rest and stress images, making each person their own control, with a probabilistic classification algorithm to quantify both stress-induced ischemia and infarction, the latter by considering both myocardial counts and regional myocardial function. Direct comparison of rest to stress after registration makes each person their own reference in the estimation of stress-induced ischemia. This is particularly advantageous when attenuation artifacts are present. Artifacts are usually present in both rest and stress MPS, and direct comparison will therefore improve the ability to distinguish ischemia from artifacts. Including wall thickening as a feature in the classification process was hypothesized to increase the specificity for defining infarction, by helping to distinguish infarction from artifacts (25, 26). For the patient material used in this study, the bias and variability between Segment and the visual analysis was unchanged,

regardless if the wall thickening information was included or not in the automatic analysis. In this study, the LV contour from the rest tomographic sections was used to define the LV myocardium in both the rest and the stress tomographic sections. The rest LV contour was hypothesized to be of higher quality than the stress LV contour, due to influence from potential stress-induced ischemia. This is opposite from the rest-stress analysis algorithm presented by Prasad et al. (8), where the stress contour was used to define the LV myocardium.

Study Limitations

One limitation with the proposed perfusion analysis algorithm is that it uses an affine transformation, without scaling, of the stress tomographic sections in the co-registration with the rest tomographic sections. This could potentially be an issue in patients with significant post-ischemic LV dilatation after stress when manual adjustment in the co-registration might be required. No patients in the present study needed manual correction in the co-registration. Another limitation is that this study only included MPS data generated by one camera setting and image reconstruction method. Further validation is necessary to investigate the performance of the proposed algorithm for other camera settings and reconstruction methods. In this study, we used expert readers as reference standard, and not an analysis method independent of MPS, like coronary angiography or PET. However,

the aim of the algorithm is to emulate the manual interpretation of myocardial perfusion analysis by MPS, and to provide support to physicians reporting MPS studies.

Conclusions

The proposed algorithm can detect and quantify stress-induced ischemia and infarction in MPS with good agreement to expert readers, and quantify stress-induced ischemia with good agreement to simulated values by a computer phantom. Hence, the proposed algorithm shows potential to provide clinically relevant quantification of perfusion defects by MPS.

Acknowledgements

The authors would like to thank technicians at Department of Clinical Physiology at Skåne University Hospital in Lund for invaluable help with data acquisition, and Shahnaz Akil for help with data analysis. Financial support was provided by Swedish Heart Lung Foundation, Lund University Faculty of Medicine, the Swedish Research Council (grant 2008-2461, 2008-2949, 2012-4944), Swedish Knowledge Foundation (grant 2009-0080), and Region of Scania.

Appendix

Automatic Perfusion Algorithm

Count Normalization

The count normalization aims to compensate for both the underestimated counts in the basal and apical part of the LV (due to thinner myocardial wall in these regions), as well as the relative nature of the counts in MPS images. The compensation method used here has been used before in an algorithm for quantification of myocardium at risk in MPS (17). The underestimation of counts in the basal part of the LV was compensated in each basal slice, defined as the slices with outflow tract by the LV segmentation. The compensation was performed by normalization of the highest count in the myocardium in each basal slice to the highest count in the whole LV myocardium. The normalization factor for the apex was calculated as the mean of the normalization factors in the two most basal slices. The apex cannot be used to set the normalization factor since apical defects might result in complete absence of counts in the apex. The relative nature of the counts in MPS images was compensated by normalization to the maximum count within the LV myocardium for each set of tomographic sections.

Image Registration

As a first step in the image registration process, the LV contours were used to place the stress image LV center at the rest image LV center. Iterative

image registration was then performed using the Simplex optimization algorithm (27). The iterative registration algorithm is based on maximization of the normalized mutual information (NMI) between the rest and the stress tomographic sections by performing an affine 3-dimensional transformation of the stress image. The transformation includes six parameters, three for translation and three for rotation of the stress tomographic sections. The NMI measures the mutual dependence of two variables and is described by Studholme et al. (28). In short, the NMI calculation starts by grouping the counts in each set of tomographic sections into bins and then calculating the NMI from the similarity between corresponding voxel counts and the occurrence of the grouped bins. In this study, the image counts for each set of tomographic sections were grouped into 50 bins according to their values.

Training of the Classification Algorithm

The training of the classification algorithm started by count normalization and image registration of the rest and the stress image stacks, for the patients in the training set. This was followed by determination of four myocardial features; rest and stress counts, rest-stress count change, and rest wall thickening, for each myocardial voxel. The rest wall thickening was calculated in the gated rest image stack and by interpolation assign to each ungated myocardial voxel. Thereafter, each voxel was assigned to one of the

three classes; normal myocardium, stress-induced ischemia or infarction. The class assignment was performed by interpolating the visual scoring values over the myocardium and assigning the voxels with a rest-stress difference score greater than 1 as stress-induced ischemia, and the voxels with an infarct score greater than 1 as infarction. The myocardial features together with the class identity, determined by the expert reader, were used as input to the training of the classification algorithm. The classification algorithm was a Naive Bayes classifier, which are based on applying Bayes' theorem with strong independence assumptions. The parameters estimated during the training were the class prior probabilities, *p(C)*, and the probability distributions, *p(F|C)*, where *F* are the features and *C* the classes. These parameters were then used in the segmentation of the perfusion defects in the test set, as described in the next section.

Classification algorithm

The measured values of the features were used to classify each myocardial voxel by the Naive Bayes classifier into one of three classes; normal, stress-induced ischemia or infarction. The classification was performed by calculating the three class probabilities for each voxel by

$$p(C_i|F_1, \ldots, F_n) = p(C_i)\prod_{j=1}^{n} p(F_j|C_i)$$

where n is the number of features and i is the class number. The values of $p(C)$ and $p(F|C)$ derives from the training of the classifier. From the probabilities, the perfusion defect segmentation was performed by assign each myocardial voxel to the class with the highest computed probability.

Refinement of the segmentation

The perfusion defect segmentation derived from the probabilistic classification was then refined based on *a priori* knowledge of perfusion defect propagations, established in a previous study (17), as follows. Segmented regions with a volume less than 5 % of the LV were considered to be noise and removed from the segmentation. Regions in the myocardium less than 1 cm^2 in a short-axis slice, which were completely surrounded by voxels included in the segmentation, were made part of the segmented region. Any region that did not approach the endocardium, as determined by the centerline method (29), were filled in the endocardial direction, based on the expected propagation of perfusion defects from endocardium to epicardium.

References

(1) Sciagra R, Leoncini M. Gated single-photon emission computed tomography. The present-day "one-stop-shop" for cardiac imaging. Q J Nucl Med Mol Imaging 2005;49:19-29.

(2) Underwood SR, Anagnostopoulos C, Cerqueira M, Ell PJ, Flint EJ, Harbinson M et al. Myocardial perfusion scintigraphy: the evidence. European journal of nuclear medicine and molecular imaging 2004;31:261-91.

(3) Gibbons RJ, Miller TD, Christian TF. Infarct size measured by single photon emission computed tomographic imaging with (99m)Tc-sestamibi: A measure of the efficacy of therapy in acute myocardial infarction. Circulation 2000;101:101-8.

(4) Itti E, Klein G, Rosso J, Evangelista E, Monin JL, Gueret P et al. Assessment of myocardial reperfusion after myocardial infarction using automatic 3-dimensional quantification and template matching. J Nucl Med 2004;45:1981-8.

(5) Okuda K, Nakajima K, Hosoya T, Ishikawa T, Matsuo S, Kawano M et al. Quantification of myocardial perfusion SPECT using freeware package (cardioBull). Annals of nuclear medicine 2011;25:571-9.

(6) Slomka PJ, Hurwitz GA, Stephenson J, Cradduck T. Automated alignment and sizing of myocardial stress and rest scans to three-dimensional normal templates using an image registration algorithm. J Nucl Med 1995;36:1115-22.

(7) Slomka PJ, Nishina H, Berman DS, Akincioglu C, Abidov A, Friedman JD et al. Automated quantification of myocardial perfusion SPECT using simplified normal limits. J Nucl Cardiol 2005;12:66-77.

(8) Prasad M, Slomka PJ, Fish M, Kavanagh P, Gerlach J, Hayes S et al. Improved quantification and normal limits for myocardial perfusion stress-rest change. J Nucl Med 2010;51:204-9.

(9) Gjertsson P, Lomsky M, Richter J, Ohlsson M, Tout D, van Aswegen A et al. The added value of ECG-gating for the diagnosis of myocardial infarction using myocardial perfusion scintigraphy and artificial neural networks. Clinical physiology and functional imaging 2006;26:301-4.

(10) Segars WP, Sturgeon G, Mendonca S, Grimes J, Tsui BM. 4D XCAT phantom for multimodality imaging research. Medical physics 2010;37:4902-15.

(11) Ljungberg M, Strand SE. A Monte Carlo program for the simulation of scintillation camera characteristics. Comput Methods Programs Biomed 1989;29:257-72.

(12) Soneson H, Hedeer F, Arevalo C, Carlsson M, Engblom H, Ubachs JF et al. Development and validation of a new automatic algorithm

for quantification of left ventricular volumes and function in gated myocardial perfusion SPECT using cardiac magnetic resonance as reference standard. J Nucl Cardiol 2011;18:874-85.

(13) Cerqueira MD, Weissman NJ, Dilsizian V, Jacobs AK, Kaul S, Laskey WK et al. Standardized myocardial segmentation and nomenclature for tomographic imaging of the heart: a statement for healthcare professionals from the Cardiac Imaging Committee of the Council on Clinical Cardiology of the American Heart Association. Circulation 2002;105:539-42.

(14) Carlsson M, Hedeer F, Engblom H, Arheden H. Head-to-head comparison of a 2-day myocardial perfusion gated SPECT protocol and cardiac magnetic resonance late gadolinium enhancement for the detection of myocardial infarction. J Nucl Cardiol 2013.

(15) Germano G, Kavanagh PB, Slomka PJ, Van Kriekinge SD, Pollard G, Berman DS. Quantitation in gated perfusion SPECT imaging: the Cedars-Sinai approach. J Nucl Cardiol 2007;14:433-54.

(16) Heiberg E, Sjogren J, Ugander M, Carlsson M, Engblom H, Arheden H. Design and validation of Segment - freely available software for cardiovascular image analysis. BMC Med Imaging 2010;10:1.

(17) Soneson H, Engblom H, Hedstrom E, Bouvier F, Sorensson P, Pernow J et al. An automatic method for quantification of myocardium at risk from myocardial perfusion SPECT in patients with acute coronary occlusion. J Nucl Cardiol 2010;17:831-40.

(18) Altman DG, Bland JM. Diagnostic tests 3: receiver operating characteristic plots. BMJ (Clinical research ed 1994;309:188.

(19) Berman DS, Kang X, Slomka PJ, Gerlach J, de Yang L, Hayes SW et al. Underestimation of extent of ischemia by gated SPECT myocardial perfusion imaging in patients with left main coronary artery disease. J Nucl Cardiol 2007;14:521-8.

(20) Lomsky M, Gjertsson P, Johansson L, Richter J, Ohlsson M, Tout D et al. Evaluation of a decision support system for interpretation of myocardial perfusion gated SPECT. European journal of nuclear medicine and molecular imaging 2008;35:1523-9.

(21) Garcia EV, Cooke CD, Folks RD, Santana CA, Krawczynska EG, De Braal L et al. Diagnostic performance of an expert system for the interpretation of myocardial perfusion SPECT studies. J Nucl Med 2001;42:1185-91.

(22) Johansson L, Lomsky M, Marving J, Ohlsson M, Svensson SE, Edenbrandt L. Diagnostic evaluation of three cardiac software packages using a consecutive group of patients. EJNMMI research 2011;1:22.

(23) Lindahl D, Lanke J, Lundin A, Palmer J, Edenbrandt L. Improved classifications of myocardial bull's-eye scintigrams with computer-based decision support system. J Nucl Med 1999;40:96-101.

(24) Declerck J, Feldmar J, Goris ML, Betting F. Automatic registration and alignment on a template of cardiac stress and rest reoriented SPECT images. IEEE transactions on medical imaging 1997;16:727-37.
(25) DePuey EG, Rozanski A. Using gated technetium-99m-sestamibi SPECT to characterize fixed myocardial defects as infarct or artifact. J Nucl Med 1995;36:952-5.
(26) Fleischmann S, Koepfli P, Namdar M, Wyss CA, Jenni R, Kaufmann PA. Gated (99m)Tc-tetrofosmin SPECT for discriminating infarct from artifact in fixed myocardial perfusion defects. J Nucl Med 2004;45:754-9.
(27) Cardoso MF, Salcedo RL, de Azevedo SF. The simplex-simulated annealing approach to continuous non-linear optimization. Comput Chem Eng 1996;20:1065-80.
(28) Studholme C, Hill DLG, Hawkes DJ. An overlap invariant entropy measure of 3D medical image alignment. Pattern Recogn 1999;32:71-86.
(29) Sheehan FH, Bolson EL, Dodge HT, Mathey DG, Schofer J, Woo HW. Advantages and applications of the centerline method for characterizing regional ventricular function. Circulation 1986;74:293-305.

TABLE 1

	Training set		
	Controls	**CAD group**	**Test set**
Number of patients	90	50	352
Age (year)	60 ± 9	69 ± 9	66 ± 10
Gender (men / women)	45 / 45	25 / 25	180 / 172
LVM (g)	121 ± 21	139 ± 34	133 ± 34
EDV (ml)	141 ± 33	162 ± 65	159 ± 64
ESV (ml)	53 ± 17	79 ± 55	74 ± 56
EF (%)	63 ± 7	55 ± 13	57 ± 12
SDS ≥ 2 (%)	0	82	23
SDS LAD ≥ 2 (%)	0	52	16
SDS RCA ≥ 2 (%)	0	44	13
SDS LCx ≥ 2 (%)	0	18	6
Infarct score ≥ 2 (%)	0	52	20
Infarct score LAD ≥ 2 (%)	0	20	13
Infarct score RCA ≥ 2 (%)	0	44	13
Infarct score LCx ≥ 2 (%)	0	24	5

TABLE 1 Patient characteristics.

The LVM, EDV, ESV and EF were derived from the automatic LV segmentation, and the summed scores were generated by visual scoring. LVM = left ventricular mass, EDV = end-diastolic volume, ESV = end-systolic volume, EF = ejection fraction, SDS = summed difference score, LAD = left anterior descending artery, LCx = left circumflex artery, RCA = right coronary artery

TABLE 2

	Stress-induced ischemia	Infarction
Observer 2	2.7 ± 3.9	0.3 ± 2.9
Observer 3	3.0 ± 4.1	0.0 ± 1.6
Segment	0.7 ± 3.8	-1.3 ± 4.7
QPS	0.1 ± 5.8	3.1 ± 3.8

TABLE 2 Validation

Bias ± SD against the reference standard of visual analysis of an expert reader for the subpopulation of 40 patients included in the interobserver analysis. Note that the results by the automated algorithms, Segment and QPS, are in the same range as the interobserver variability.

TABLE 3

	Stress-induced ischemia					
	Segment			QPS		
	All	Men	Women	All	Men	Women
Threshold	3.4	3.4	2.2	2.0	1.0	3.0
Sensitivity	0.76 (0.047)	0.82 (0.057)	0.76 (0.071)	0.55 (0.055)	0.60 (0.073)	0.49 (0.082)
Specificity	0.83 (0.023)	0.82 (0.033)	0.78 (0.036)	0.69 (0.028)	0.69 (0.040)	0.68 (0.040)
Positive predictive value	0.58 (0.048)	0.61 (0.063)	0.48 (0.066)	0.35 (0.042)	0.39 (0.059)	0.30 (0.058)
Negative predictive value	0.92 (0.017)	0.93 (0.023)	0.92 (0.025)	0.83 (0.025)	0.84 (0.035)	0.83 (0.036)
Accuracy	0.82 (0.021)	0.82 (0.028)	0.77 (0.032)	0.66 (0.025)	0.67 (0.035)	0.64 (0.037)
True positive fraction	0.18 (0.020)	0.21 (0.030)	0.16 (0.028)	0.13 (0.018)	0.15 (0.027)	0.10 (0.023)
False positive fraction	0.13 (0.018)	0.13 (0.025)	0.17 (0.029)	0.24 (0.023)	0.23 (0.032)	0.25 (0.033)
True negative fraction	0.64 (0.026)	0.62 (0.036)	0.61 (0.037)	0.53 (0.027)	0.52 (0.037)	0.53 (0.038)
False negative fraction	0.06 (0.012)	0.04 (0.015)	0.05 (0.017)	0.11 (0.016)	0.10 (0.022)	0.11 (0.024)

	Infarction					
	Segment			QPS		
	All	Men	Women	All	Men	Women
Threshold	1.2	1.2	1.7	6.0	6.0	6.0
Sensitivity	0.86 (0.039)	0.87 (0.047)	0.84 (0.073)	0.82 (0.043)	0.81 (0.054)	0.84 (0.073)
Specificity	0.93 (0.016)	0.91 (0.025)	0.95 (0.018)	0.84 (0.022)	0.82 (0.034)	0.86 (0.029)
Positive predictive value	0.77 (0.045)	0.81 (0.052)	0.75 (0.082)	0.59 (0.047)	0.65 (0.059)	0.50 (0.077)
Negative predictive value	0.96 (0.012)	0.94 (0.021)	0.97 (0.014)	0.94 (0.015)	0.91 (0.026)	0.97 (0.015)
Accuracy	0.91 (0.015)	0.90 (0.022)	0.94 (0.019)	0.84 (0.020)	0.82 (0.029)	0.85 (0.027)
True positive fraction	0.19 (0.021)	0.26 (0.033)	0.12 (0.025)	0.18 (0.021)	0.24 (0.032)	0.12 (0.025)
False positive fraction	0.06 (0.012)	0.06 (0.018)	0.04 (0.015)	0.13 (0.018)	0.13 (0.025)	0.12 (0.025)
True negative fraction	0.72 (0.024)	0.64 (0.036)	0.81 (0.030)	0.65 (0.025)	0.58 (0.037)	0.73 (0.034)
False negative fraction	0.03 (0.009)	0.04 (0.014)	0.02 (0.011)	0.04 (0.010)	0.06 (0.017)	0.02 (0.011)

TABLE 3 ROC analysis

Result from the ROC analysis for the both automatic perfusion analysis algorithms Segment and QPS, by using expert reader as reference standard. The values in parentheses indicate the standard error.

FIGURE 1: The simulated MPS in female geometry with a perfusion defect in the RCA region in the stress image. The yellow arrows indicate the perfusion defect with a severity of 40 %. The white lines indicate the LV contours derived from automatic segmentation by Segment.

FIGURE 2: Illustration of the interface for manual scoring of tracer uptake (A) and presence of infarct (B). In the scoring process, three short-axis (basal, midventricular and apical) and two long-axis (horizontal and vertical) tomographic sections were shown with the 17 segment model overlaid. For the scoring of tracer uptake, the ungated rest and stress tomographic sections were used, and for the scoring of presence of infarction, the gated and ungated rest tomographic sections were used. The tracer uptake in each segment was graded using a 5-point scale (0 = normal, 1 = equivocal, 2 = moderate, 3 = severe reduction, and 4 = apparent absence). The presence of infarction was graded using a 3-point scale (0 = normal, 1 = equivocal and 2 = infarction/hibernation).

FIGURE 3: Relationship between the simulated TPD by the computer phantom and the D-TPD measured by Segment (upper panels) and QPS (lower panels). In the left panels the dashed line is the line of identity, and the solid line is the linear regression line. In the right panels the solid line is the mean bias and the dashed lines 2 SD. Please note some symbols have been superimposed.

D-TPD = difference total perfusion deficit

FIGURE 4: Relationship between visual scoring by the expert reader and perfusion defect quantification by Segment. In the left panel the solid line is the linear regression line. In the

right panel the solid line is the mean bias and the dashed lines 2 SD. Please note some symbols have been superimposed.

SD%, SR% = visual perfusion scoring for stress-induced ischemia and infarction, respectively, D-TPD, R-TPD = total perfusion deficit for stress-induced ischemia and infarction, respectively

FIGURE 5: Relationship between visual scoring by the expert reader and perfusion defect quantification by QPS. In the left panel the solid line is the linear regression line. In the right panel the solid line is the mean bias and the dashed lines 2 SD. Please note some symbols have been superimposed.

SD%, SR% = visual perfusion scoring for stress-induced ischemia and infarction, respectively, D-TPD, R-TPD = total perfusion deficit for stress-induced ischemia and infarction, respectively

FIGURE 6: The upper left panel shows the distribution of the TPD quantification by Segment for the patients with normal myocardial perfusion for stress-rest difference by the expert reader (SD% = 0). The upper right panel shows the distribution of the TPD quantification by Segment for the patients with normal myocardial perfusion at rest by the expert reader (SR% = 0). The lower panels show the corresponding plots for the TPD quantification by QPS.

TPD = total perfusion deficit, SD%, SR% = visual perfusion scoring for stress-induced ischemia and infarction, respectively

FIGURE 7: Results from the image registration and perfusion defect quantification by Segment in one patient with both stress-induced ischemia and infarction. The white lines

indicate the LV segmentation derived from the rest tomographic sections and transferred to the aligned stress image. The yellow lines indicate the perfusion defect segmentation. Stress-induced ischemia was measured to D-TPD = 11 by Segment and SD% = 14 by the expert reader. Infarction was measured to R-TPD = 4 by Segment and SR% = 5 by the expert reader. SD%, SR% = visual perfusion scoring for stress-induced ischemia and infarction, respectively, D-TPD, R-TPD = total perfusion deficit for stress-induced ischemia and infarction, respectively

FIGURE 8: ROC curve of diagnostic accuracy for TPD by Segments to detect stress-induced ischemia and infarction, respectively, compared to the reference standard visual scoring by the expert reader. The blue circles indicate the point on the ROC curve closest to the upper left corner, and the corresponding TPD threshold and statistical analysis results are presented in Table 3. The values in parentheses indicate the standard error of the AUC.
TPD = total perfusion deficit, AUC = area under curve

SUPPLEMENTAL FIGURE 1: ROC curve of diagnostic accuracy for TPD by QPS to detect stress-induced ischemia and infarction, respectively, compared to the reference standard visual scoring by the expert reader. The blue circles indicate the point on the ROC curve closest to the upper left corner, and the corresponding TPD threshold and statistical analysis results are presented in Table 3. The values in parentheses indicate the standard error of the AUC.
TPD = total perfusion deficit, AUC = area under curve

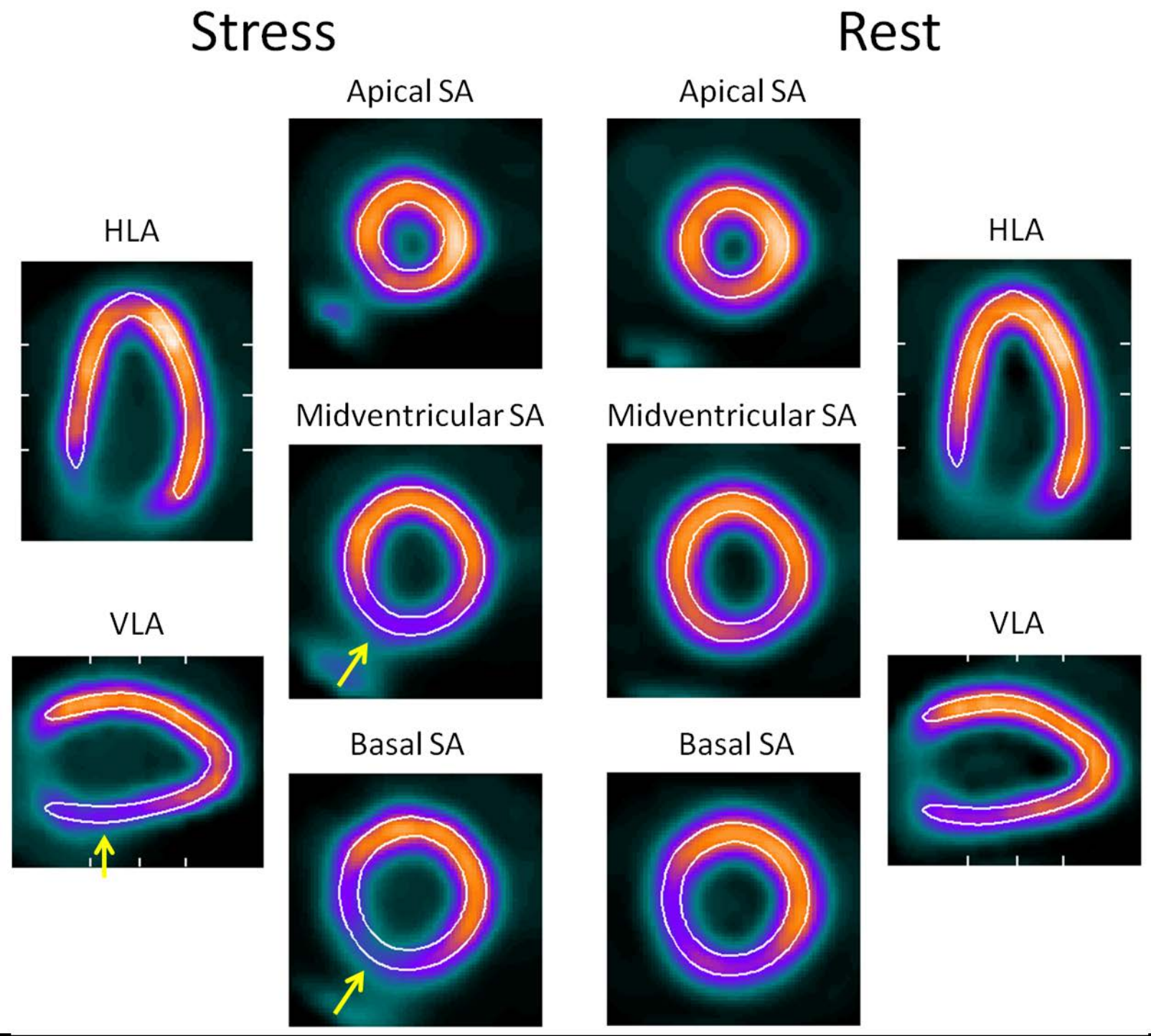
Stress
Rest
Apical SA
Apical SA
HLA
HLA
Midventricular SA
Midventricular SA
VLA
VLA
Basal SA
Basal SA

A

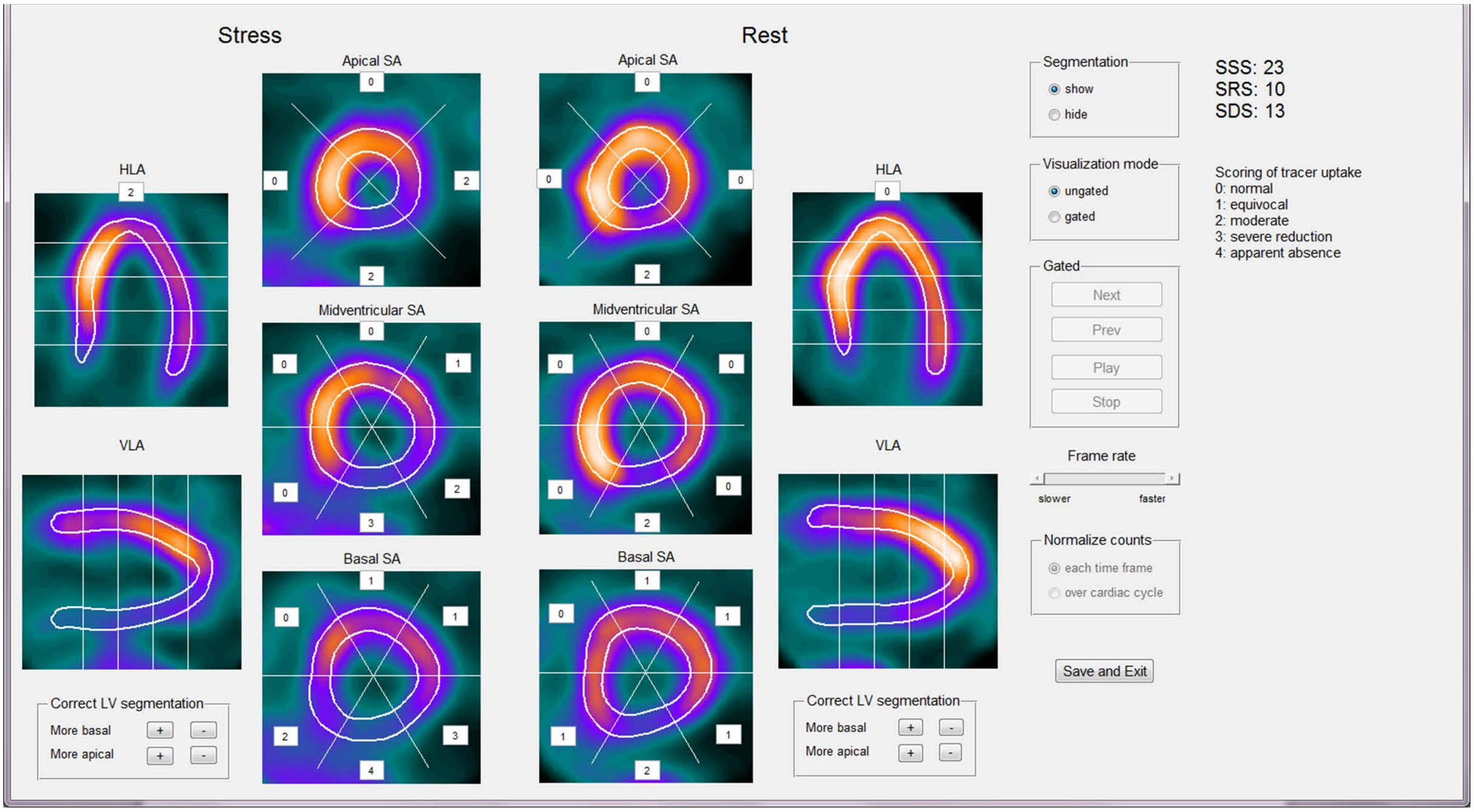
Stress
Rest
Apical SA
Midventricular SA
Basal SA
HLA
VLA
Correct LV segmentation
More basal
More apical
Segmentation
show
hide
Visualization mode
ungated
gated
Gated
Next
Prev
Play
Stop
Frame rate
slower
faster
Normalize counts
each time frame
over cardiac cycle
Save and Exit
SSS: 23
SRS: 10
SDS: 13
Scoring of tracer uptake
0: normal
1: equivocal
2: moderate
3: severe reduction
4: apparent absence

B

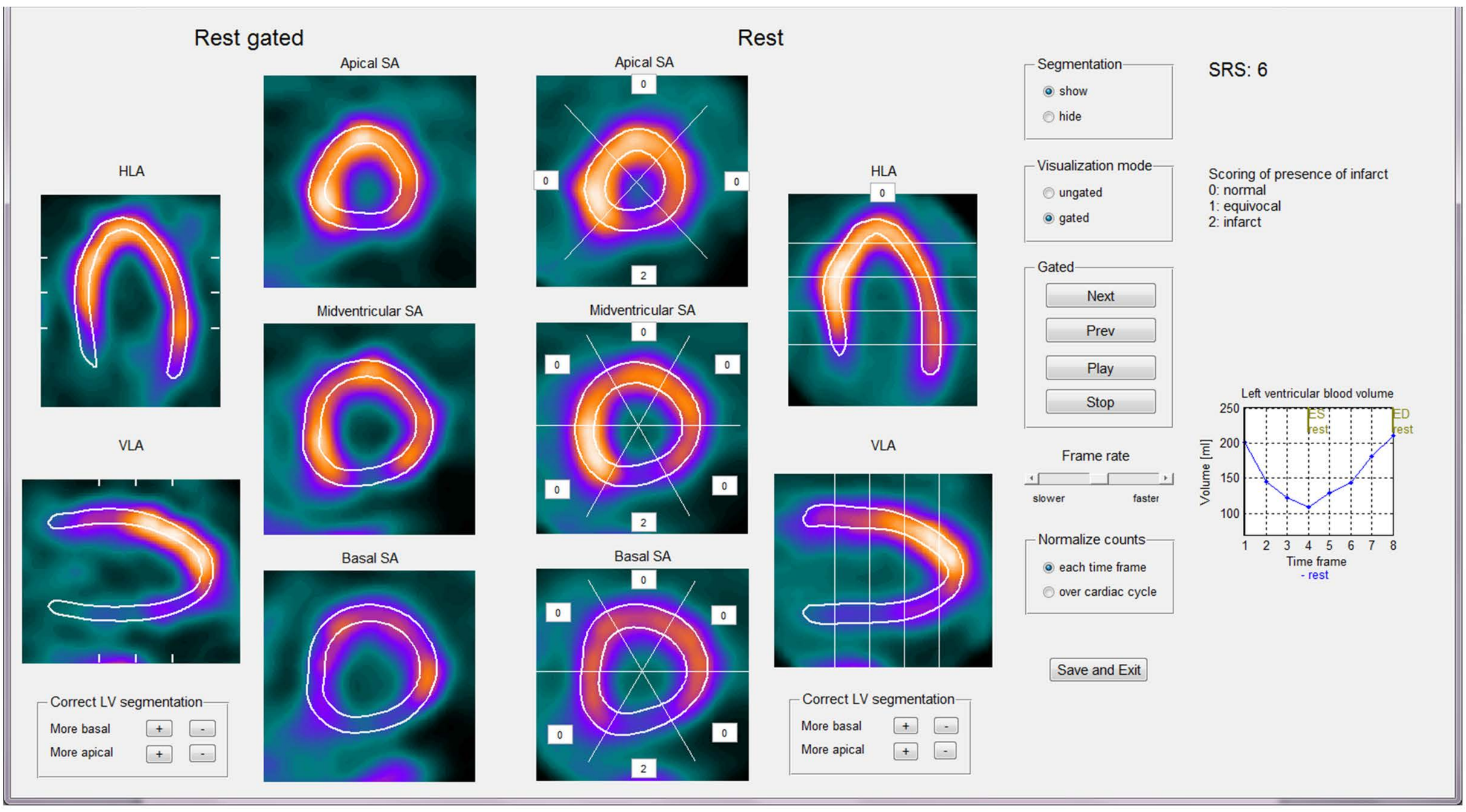
Rest gated
Rest
Apical SA
Midventricular SA
Basal SA
HLA
VLA
Correct LV segmentation
More basal
More apical
Segmentation
show
hide
Visualization mode
ungated
gated
Gated
Next
Prev
Play
Stop
Frame rate
slower
faster
Normalize counts
each time frame
over cardiac cycle
Save and Exit
SRS: 6
Scoring of presence of infarct
0: normal
1: equivocal
2: infarct
Left ventricular blood volume
Volume [ml]
Time frame
- rest
ES
ED

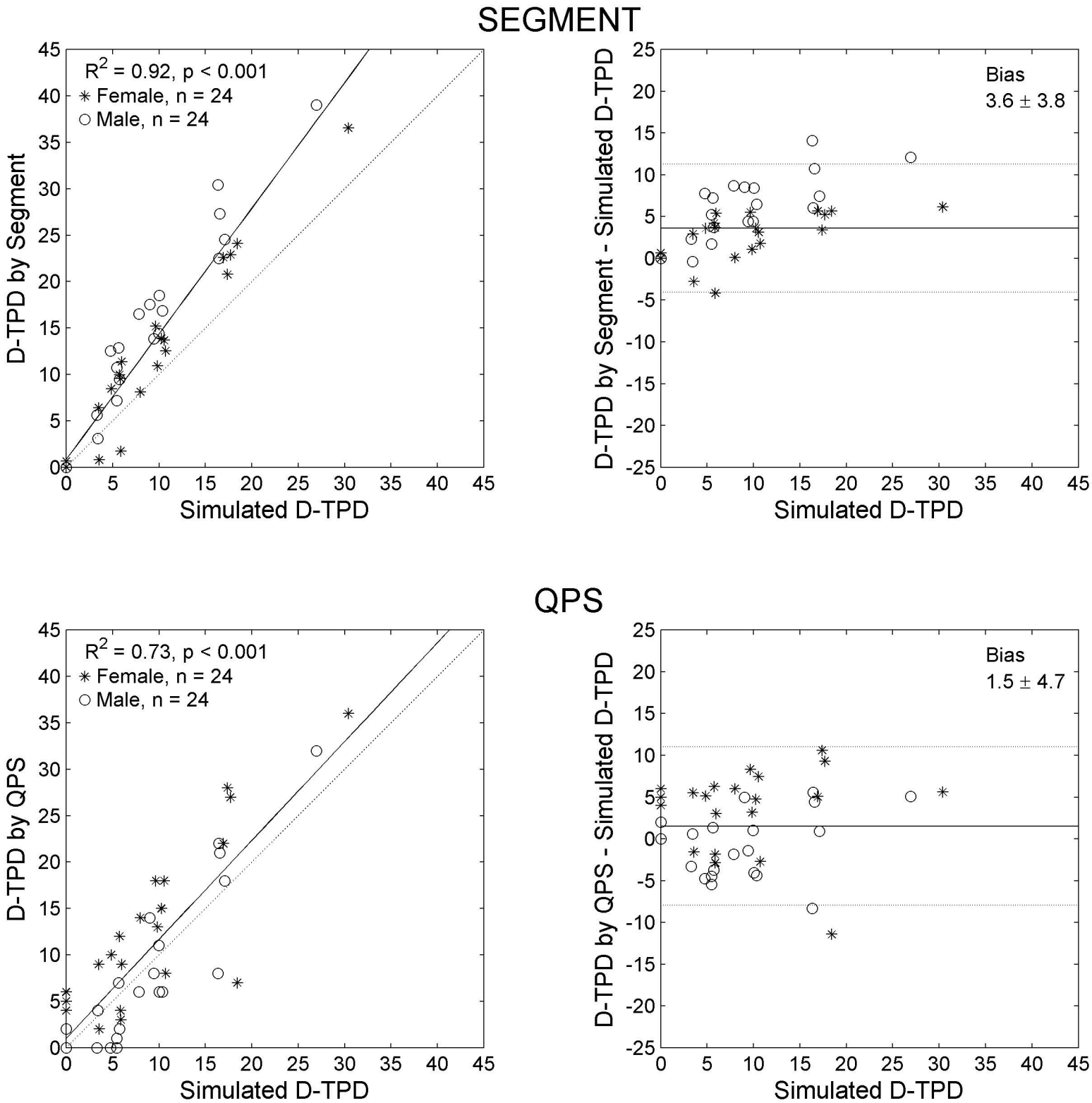
SEGMENT
R^2 = 0.92, p < 0.001
Female, n = 24
Male, n = 24
D-TPD by Segment
Simulated D-TPD
Bias
3.6 ± 3.8
D-TPD by Segment - Simulated D-TPD
Simulated D-TPD
QPS
R^2 = 0.73, p < 0.001
Female, n = 24
Male, n = 24
D-TPD by QPS
Simulated D-TPD
Bias
1.5 ± 4.7
D-TPD by QPS - Simulated D-TPD
Simulated D-TPD

SEGMENT

Stress-induced ischemia

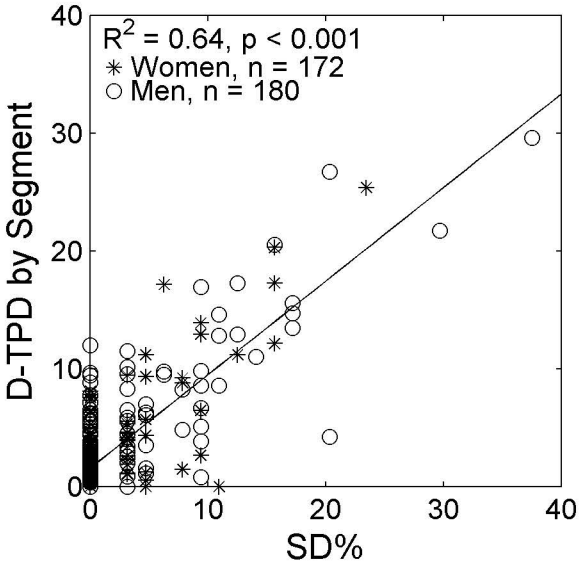

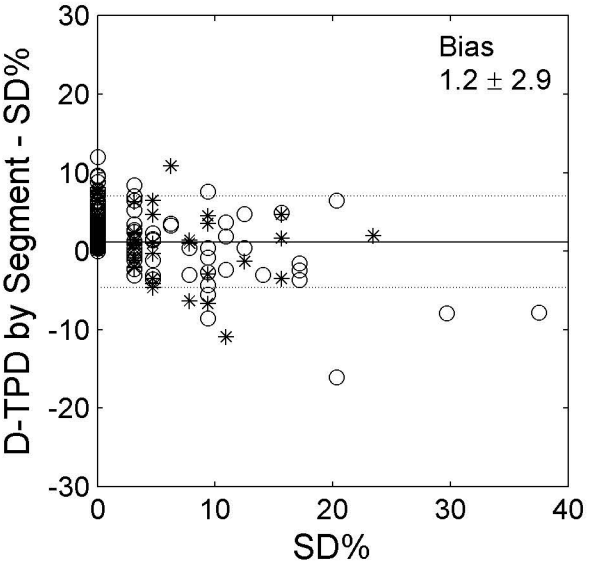

Infarction

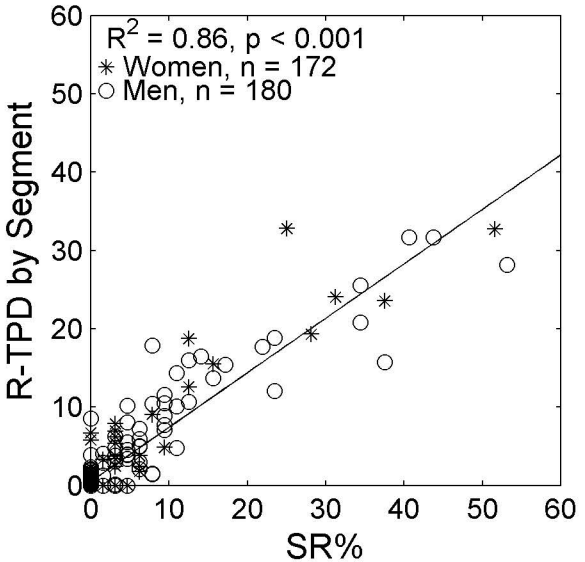

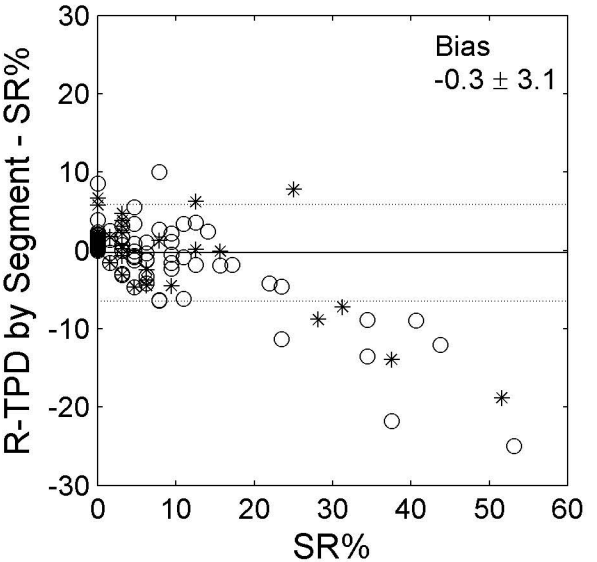

QPS

Stress-induced ischemia

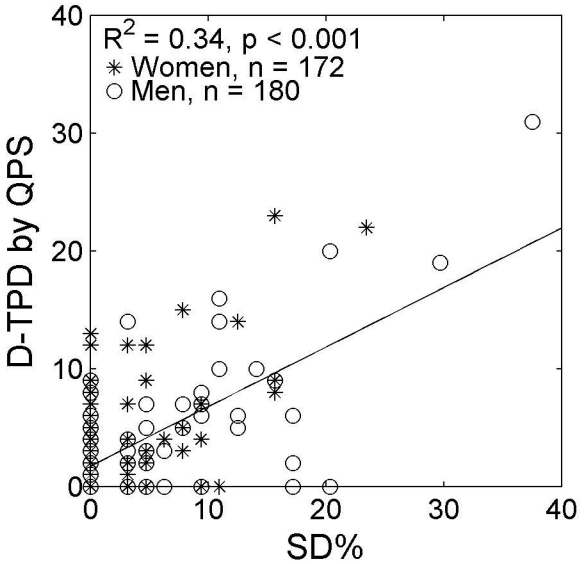

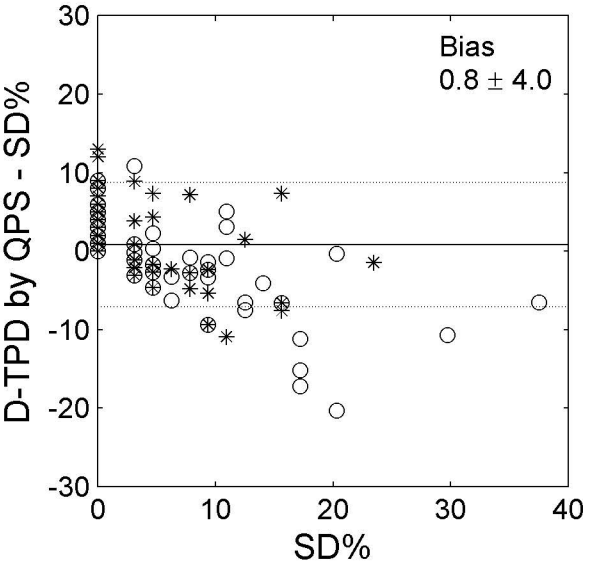

Infarction

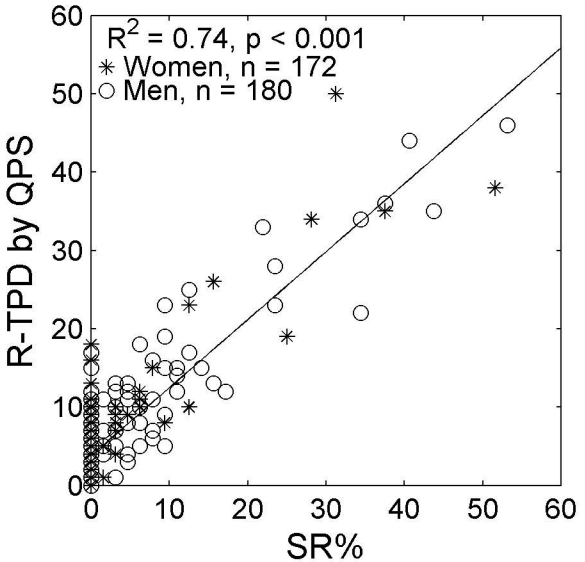

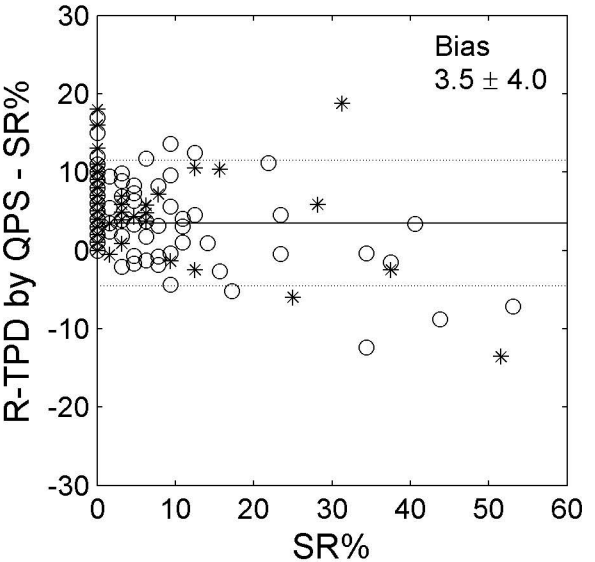

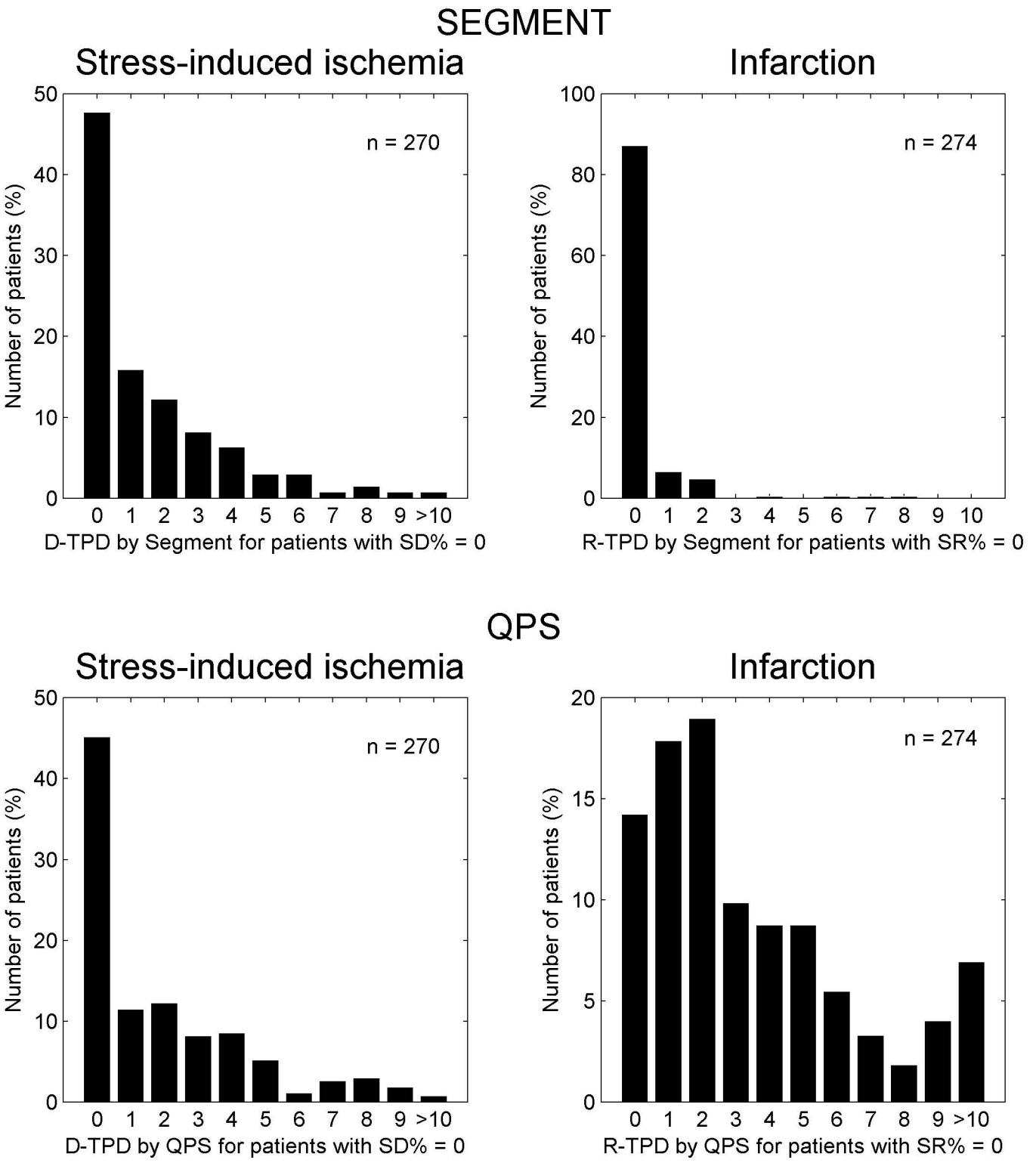
SEGMENT
Stress-induced ischemia
Infarction
n = 270
n = 274
Number of patients (%)
0 1 2 3 4 5 6 7 8 9 >10
0 1 2 3 4 5 6 7 8 9 10
D-TPD by Segment for patients with SD% = 0
R-TPD by Segment for patients with SR% = 0
QPS
Stress-induced ischemia
Infarction
n = 270
n = 274
Number of patients (%)
0 1 2 3 4 5 6 7 8 9 >10
0 1 2 3 4 5 6 7 8 9 >10
D-TPD by QPS for patients with SD% = 0
R-TPD by QPS for patients with SR% = 0

Stress

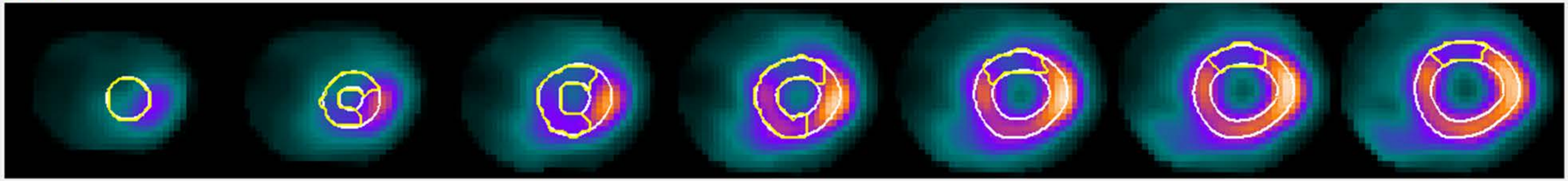

Rest

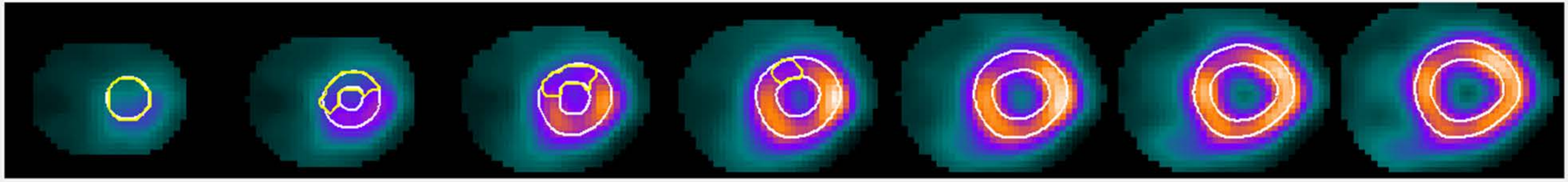

Stress

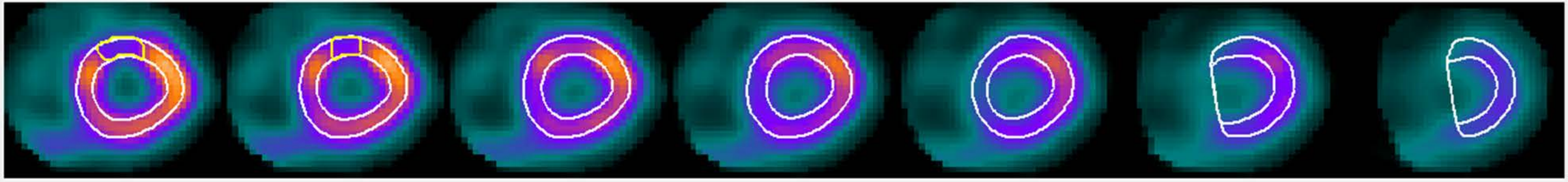

Rest

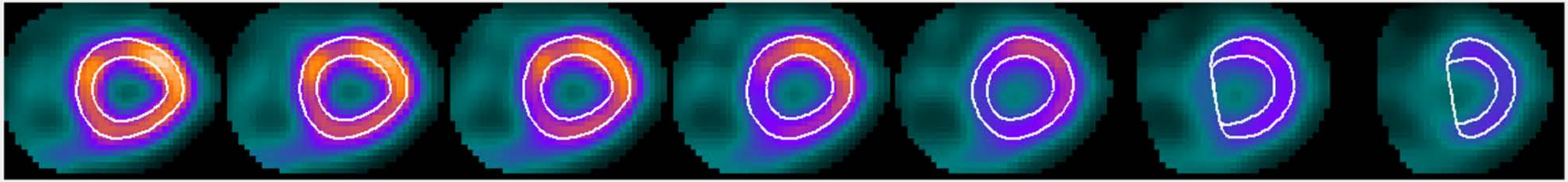

SEGMENT

Stress-induced ischemia

Infarction

All

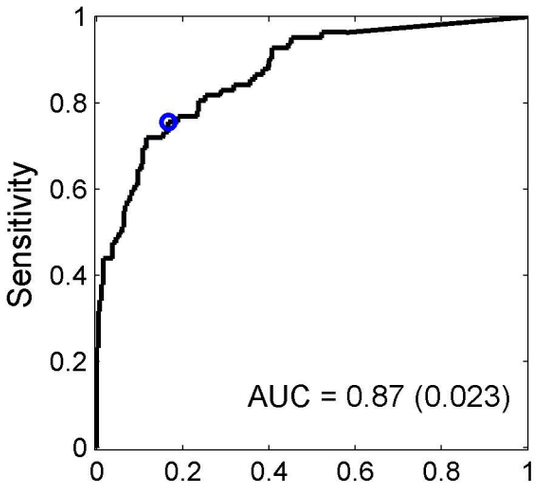

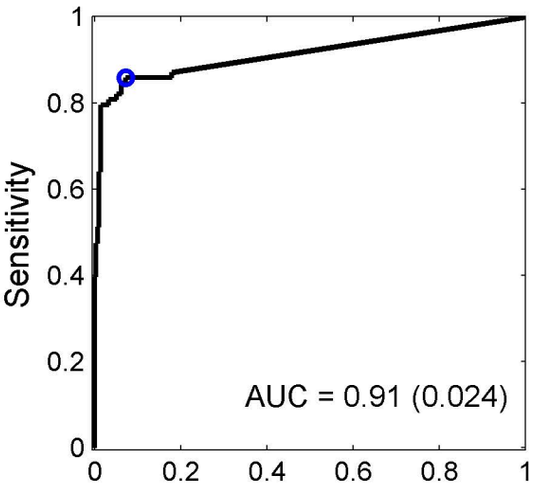

Men

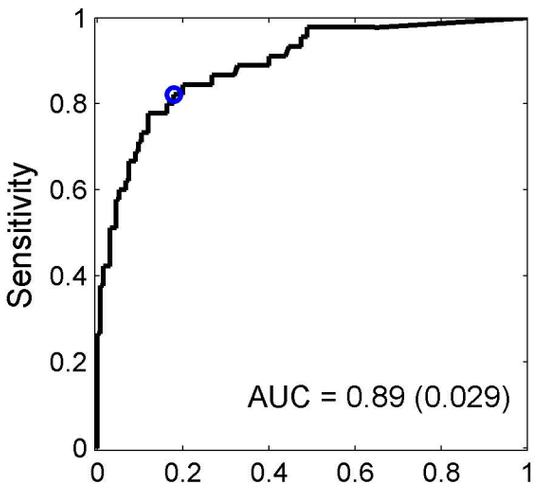

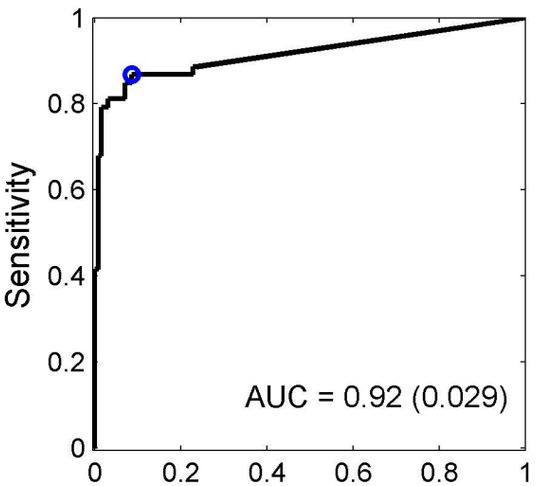

Women

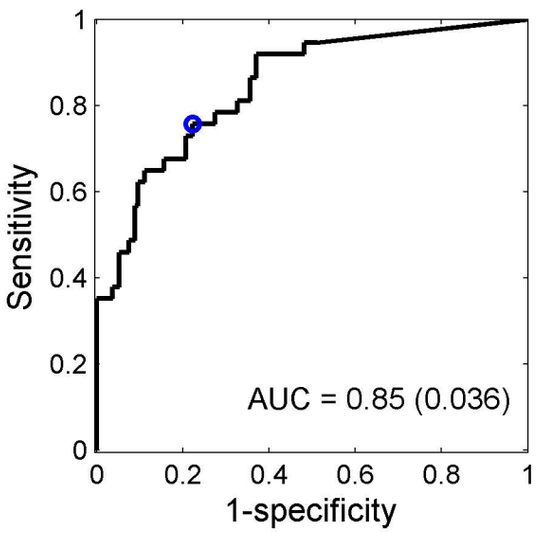

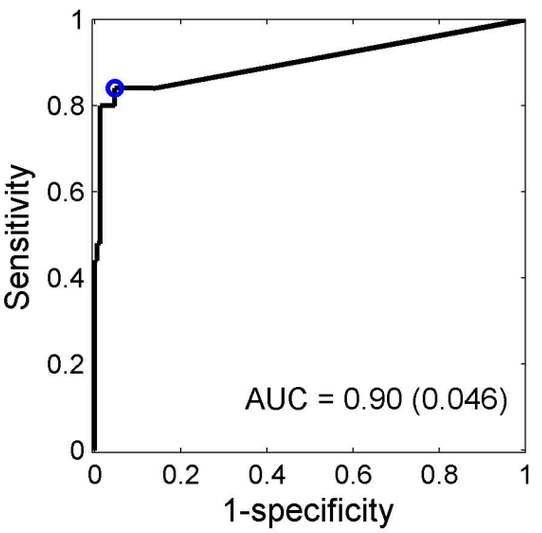

QPS

Stress-induced ischemia

Infarction

All

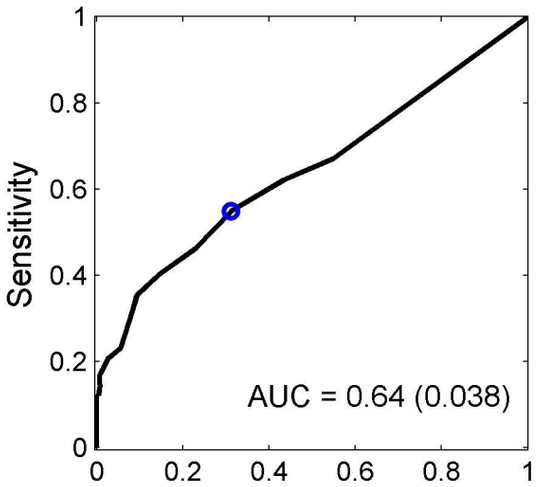

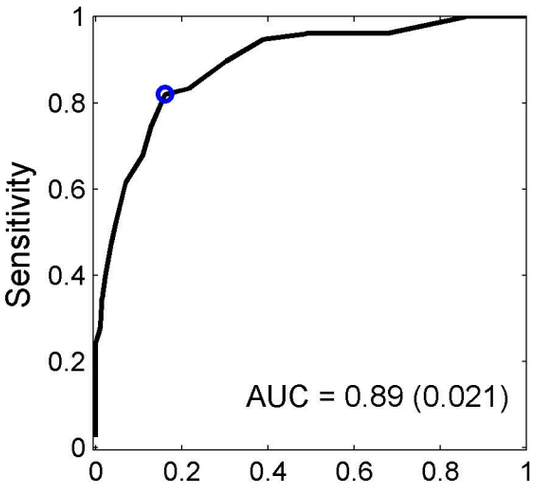

Men

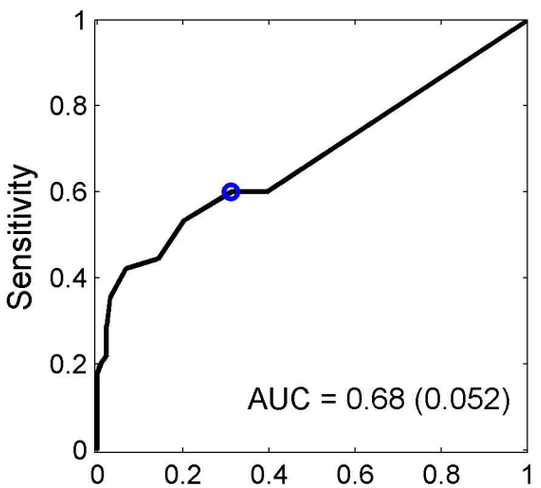

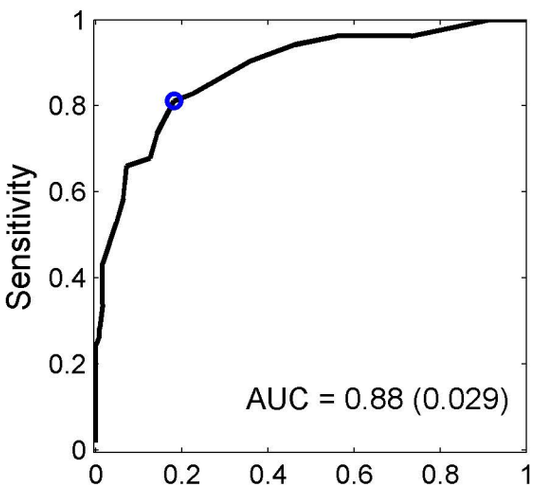

Women